minerals

MDPI

Article

Ti-Magnetite Crystallization in Melt Inclusions of Trachytic Rocks from the Dokdo and Ulleung Islands, South Korea: Implications for Hydrous and Oxidized Magmatism

Inkyeong Moon [1,2], Hyunwoo Lee [2,*], Jonguk Kim [1], Jihye Oh [1], Donghoon Seoung [3], Chang Hwan Kim [4], Chan Hong Park [4] and Insung Lee [2]

1 Deep–Sea and Seabed Mineral Resources Research Center, Korea Institute of Ocean Science and Technology, Busan 49111, Korea; moonik@kiost.ac.kr (I.M.); jukim@kiost.ac.kr (J.K.); glauxo@kiost.ac.kr (J.O.)
2 School of Earth and Environmental Sciences, Seoul National University, Seoul 08826, Korea; insung@snu.ac.kr
3 Faculty of Earth Systems and Environmental Sciences, Chonnam National University, Gwangju 61186, Korea; dseoung@jnu.ac.kr
4 East Sea Research Institute, Korea Institute of Ocean Science and Technology, Uljin 36315, Korea; kimch@kiost.ac.kr (C.H.K.); chpark@kiost.ac.kr (C.H.P.)
* Correspondence: lhw615@snu.ac.kr; Tel.: +82-2-880-6732

Received: 7 July 2020; Accepted: 20 July 2020; Published: 20 July 2020

Abstract: The Dokdo and Ulleung islands (Korea) are volcanic islands in the East Sea (Sea of Japan), formed in the late Cenozoic. These volcanic islands, in the back-arc basin of the Japanese archipelago, provide important information about magma characteristics in the eastern margin of the Eurasian plate. The origin of the Dokdo and Ulleung intraplate volcanism is still controversial, and the role of fluids, especially water, in the magmatism is poorly understood. Here, we comprehensively analyzed the melt inclusions (10–100 μm in diameter) hosted in clinopyroxene phenocrysts of trachyte, trachyandesite, and trachybasalt. In particular, we observed Ti-magnetite and amphibole which were crystallized as daughter mineral phases within melt inclusions, suggesting that Ti-magnetite was formed in an oxidized condition due to H_2O dissociation and H_2 diffusion. The Ti-magnetite exhibited compositional heterogeneities of MgO (average of 8.28 wt %), Al_2O_3 (average of 8.68 wt %), and TiO_2 (average of 8.04 wt %). The positive correlation of TiO_2 with Cr_2O_3 is probably attributed to evolutionary Fe–Ti-rich parent magma. Correspondingly, our results suggested hydrous and oxidized magmatism for the Dokdo and Ulleung volcanic islands.

Keywords: Dokdo and Ulleung islands; late Cenozoic volcanic islands; Fe-rich melt inclusion; Ti-magnetite; hydrous magmatism

1. Introduction

The Dokdo and Ulleung islands (DUI) are volcanoes located in the East Sea (Sea of Japan) that are a back-arc basin between the Korean peninsula and the Japanese arc, formed in the late Cenozoic (Figure 1a). The volcanic rocks of DUI provide an ideal opportunity to understand the evolved alkaline magmatism in the eastern margin of the Eurasian plate [1].

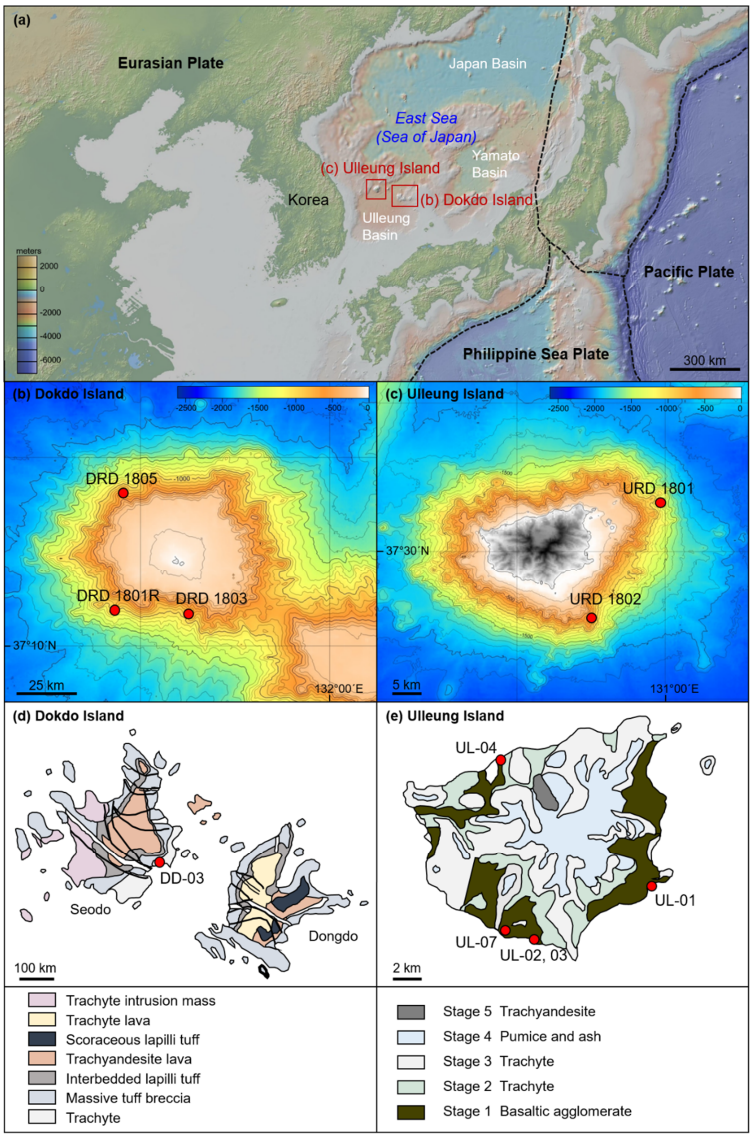

Figure 1. (**a**) Geological map of the Dokdo and Ulleung islands (DUI) with the distribution of adjacent plates (GeoMapApp 3.6.10). Contour maps of (**b**) Dokdo and (**c**) Ulleung generated using SURFER software. Contour interval is 100m. (**d**,**e**) Distribution of Late Cenozoic volcanic rocks from DUI [2]. (**b**,**c**) Submarine and (**d**,**e**) terrestrial sampling locations marked on map with solid red circles.

Previous studies primarily focused on the topography, geology, petrology, mineralogy, and geochemistry of the volcanic rocks to investigate the DUI evolutionary processes [1–12]. From these studies, Choi et al. [3], Brenna et al. [1], and Chen et al. [2] reported the genesis and evolution of primitive DUI magma mainly on the basis of geochemical, isotopic, and geochronological results. According to these studies, Ulleung island is an intraplate volcano and evolved through four eruption stages: (1) 1.37–0.97 Ma, (2) 0.83–0.77 Ma, (3) 0.73–0.24 Ma, and (4) ~20 ka. Two compositionally different parental magma types (trachytic and phonolitic magma) were recorded. Polygenic volcanism was generated using deep plumbing systems with episodic intervals. Dokdo also formed via intraplate alkali volcanism, and volcanic rocks date from the early Pliocene (4.6 ± 0.4 Ma) to the late Pliocene and Quaternary (2.7 ± 0.1 Ma) [11]. The authors also discuss in detail the geochemical properties of crystal fractionation from alkaline basaltic magma and a magmatic plumbing system beneath DUI in the Late Cenozoic [2]. The magmatic plumbing system of DUI is composed of at least two magma reservoirs at different levels, and evolved by multistage magma ascent (between 20 and 100 km). The ascent magma was situated at shallower depth before eruption.

The mantle-originated basaltic magma of DUI exhibited similar geochemical features, including high $^{87}Sr/^{86}Sr$ and low $^{143}Nd/^{144}Nd$ ratios, and indicating mixing between depleted mid-ocean ridge basalt mantle (DMM) and enriched mantle 1 (EM1) [3,13,14]. In particular, Chen et al. [2] provided geochemical evidence for magma evolutionary processes of the oceanic subducting crust with the role of DUI fluids. The existence of fluids in the magma source was also identified by several lines of evidence [15–18]. First, large ion lithophile elements (LILE: K, Rb, Sr, and Ba) are much more enriched than high-field-strength elements (HFSEs) and rare earth elements (REEs). Second, there are negative correlations between Ba/Th, Sr/Th, Ba/La, and Th/Nd. Third, alkalis such as K_2O (~7.32 wt %) and Na_2O (~5.47 wt %) show relatively high concentrations. In addition to chemical compositions, the coexisting ilmenite and magnetite indicate the exsolution of ilmenite from magnetite occurring at the subsolidus-alteration stages. Water contents were 3–4 wt % for trachytes, 3.5–7 wt % for phonolites, and 5–8 wt % for the phaneritic lithics of Ulleung based on calculated oxygen fugacity [19–21]. The presence of fluids in DUI magma is significant to examine the interaction of the subducting Pacific Plate and the mantle components beneath the DUI region. Although some previous studies suggested the presence of water in the magmatic system of DUI, the role of fluids, especially water, in the deep magmatic system of DUI is poorly known [2].

From this perspective, we investigated the geochemical properties of melt inclusions in DUI volcanic rocks for further evaluation. Melt inclusions are small droplets of melts trapped during crystallization that can be used as a geochemical proxy to track magma sources and evolution [22]. In detail, they are widely used as tracers of the physicochemical evolution of magmatic systems, mantle composition, trapping temperature, cooling rate, magma-chamber processes, and volatile contents [22]. Some previous studies examined daughter minerals within the melt inclusion to understand phenomena, such as magma evolution [23], fractionation of Fe–Ti-rich melts [24], silicate–carbonate liquid immiscibility [25], and mantle mixing [26]. Particularly, the assemblages of daughter minerals in melt inclusions with their chemical compositions can constrain the evolutionary processes of magma and the physicochemical properties of magma sources [24,27]. Melt inclusions have been utilized to investigate the petrogenesis, but the lack of developed analytical techniques prevented the observation of the limit size of melt inclusions [28]. In order to overcome this problem, we used analytical tools such as Raman spectroscopy, field-emission scanning electron microscopy (FE-SEM), and field-emission electron-probe microanalysis (FE-EPMA). As the first study on melt inclusions in DUI volcanic rocks, we seek here to identify the role of fluids in relation to the origin of DUI magma through analysis of daughter minerals.

2. Geological Background

The East Sea (Sea of Japan) is a back-arc basin of the Japanese arc that comprises the Ulleung, Yamato, and Japan basins (Figure 1a) [29]. DUI volcanoes, which have intraplate affinity, developed magmatic plumbing systems, and were produced by multistage volcanic eruptions [9,11,12,30]. The East Sea is a semimarginal basin and the opening mode has been debated for several decades [31–36]. The East Sea opening first occurred because of thinning in the crust of the northeastern Japan basin in the Early Oligocene (ca. 32 Ma), and the sea-floor spreading toward the southwest in the Late Oligocene (ca. 28 Ma). Sea-floor spreading finally terminated in the late Early Miocene (ca. 18 Ma) [35,37]. During these periods, the East Sea was extended, and the Yamato and Ulleung basins were formed [35,37]. In the Late Miocene, the mode of plate movement changed to subduction along the east and southeast of the Japanese islands, which was followed by back-arc closure and crustal shortening [38]. The Ulleung basin is considered an immature back-arc basin due to the closure of the back-arc opening [39,40]. Dokdo is located in the northern part of the Ulleung basin in the East Sea (Sea of Japan), and includes Dongdo (east islet) and Seodo (west islet) (Figure 1a,b,d). The islets rise approximately 2000 m above the sea floor [11] and comprise trachybasalts, trachytes, trachyandesite lava flows, and pyroclastic rocks (Figure 1d) [8,11]. The majority of the pyroclastic rocks in Dokdo were produced between 2.7 and 2.1 Ma [11]. Four stages of volcanic eruptions are proposed on the basis of lithofacies: subaqueous

stage (Transitional Stage 1); Surtseyan eruptive phase (Transitional Stage 2); Taalian eruptive phase; and subaerial stage [41–43]. Ulleung is located off the eastern coast of the Korean peninsula on the northern margin of Ulleung basin (Figure 1c,e) [12,44–46]. The island (ca. 30 km in diameter at its base) rises 3000 m above the sea floor (Figure 1c). Volcanic eruptions consisted of four stages from the Pleistocene (~1.4 Ma) to the middle Holocene (~5 ka) [12,44–46]. The first stage (1.37–0.97 Ma) produced the Dodong basalts, including basaltic-lava sequences and pyroclastic deposits. Trachytes that show vertical fan-shaped flow structures erupted during the second (0.83–0.77 Ma) and third (0.73–0.24 Ma) stages. A sequence of caldera eruptions occurred during the fourth stage (18.8, 8.4, and 5.6 ka) [1].

3. Analytical Methods

The major-element compositions in submarine DUI rocks were determined by X-ray fluorescence spectrometry (SHIMADZU XRF-1700) at Pukyong National University, Busan, Korea. Daughter-mineral phases in the melt inclusion were identified using in situ micro-Raman analysis (RAMAN spectrometer II, DXR2xi), FE-SEM (SUPRA 55VP), and FE-EPMA (JXA-8530F) on polished thin sections. The Raman measurements were performed at the National Center for Interuniversity Research Facilities (NCIRF) at Seoul National University (SNU), Seoul, Korea with the following settings: laser wavelength = 532 nm; laser power = 5.0 mW; exposure time = 0.005 s; number of scans = 800; the detector was an electron-multiplying charge-coupled device (EM CCD). The Raman signal was collected from 50 to 3500 cm^{-1}. The FE-SEM at the National Instrumentation Center for Environmental Management (NICEM) at SNU was used to identify mineral compositions and perform element mapping (Si, Mg, Fe, Al, Ca, and Na). The polished thin sections were coated with platinum using a BAL-TEC/SCD 005 sputter coater (20 mA and 700 s). Energy-dispersive spectroscopy (EDS) was performed with an accelerating voltage of 15 kV, a working distance of 8.4 mm, and a magnification of 5000×. Major-element concentrations of daughter-mineral phases in the melt inclusions were quantified using FE-EPMA at NCIRF, SNU. Operating conditions were accelerating voltage = 15 kV; beam current = 20 nA; beam size = 3 μm; working distance = 10.5 mm; and counting time = 10 s for Na and K, and 20 s for Mg, Si, Al, Fe, Mn, Cr, Ti, and Ca.

4. Results

4.1. Sample Description

Submarine volcanic rocks were dredged by the East Sea Exploration (Onnuri R/V) for the Korea Institute of Ocean Science and Technology (KIOST) in 2018 (Figure 1b,c). Samples were collected near the Dokdo and Ulleung islands at depths of approximately 1000 m (Figure 1b,c). Rock samples were relatively fresh with a massive texture. At the DRD-1801R site sampled from the southwestern slope of Dokdo, trachytic rocks were mainly obtained. In DRD-1802, which was sampled at a shallow water depth of the southwest slope, trachytic rocks with phenocrysts were also acquired and some elongated vesicles were also observed. At the DRD-1803 site on the southern slope, trachytic rocks similar to the southwestern slope were also collected along with basement rocks with an altered surface turned yellowish. In DRD-1804, it is located on the southeast slope, and DRD-1805 was dredged with basaltic rocks in addition to trachytic rocks. In the URD-1801 on the northeastern slope of Ulleung, trachytic rocks were collected, and some massive basaltic rocks were sampled together. The URD-1802, located on the southern slope, collected only trachytic rocks, and mostly 5 mm or less of plagioclase phenocrysts were observed.

We analyzed the Dokdo submarine rocks (DRD-1801R, 1803, 1805) and the Ulleung submarine samples (URD-1801, 1802) that were phyric with 5–10 mm phenocrysts of pyroxene, olivine, and plagioclase. A trachyte (DD-03) and 5 basaltic agglomerate samples (UL-01, UL-02, UL-03, UL-04, and UL-07) were collected in Seodo (west islet of Dokdo island) (Figures 1d and 2a) and Ulleung island (Figures 1e and 2b,c), respectively. These subaqueous samples have abundant phenocrysts of pyroxene

and plagioclase up to 2 mm in diameter. Abundant melt inclusions were observed in pyroxene (augite) phenocrysts within the DUI rocks (Figure 3), consistent with previous work [1]. Olivine and plagioclase melt inclusions were not included in this study. Most melt inclusions were primary; secondary melt inclusions were excluded. Primary melt inclusions have polygonal to sub-rounded shapes, while secondary melt inclusions present trails, chains, and compact swarm shapes or are distributed in the cracks of host minerals [47,48]. Melt inclusions were round, rectangular, and irregular-shaped, with variable sizes from 10 to 100 μm in diameter. In our study, melt inclusions were divided into two subgroups on the basis of the presence or absence of daughter minerals with or without irregularly shaped voids (Figure 3).

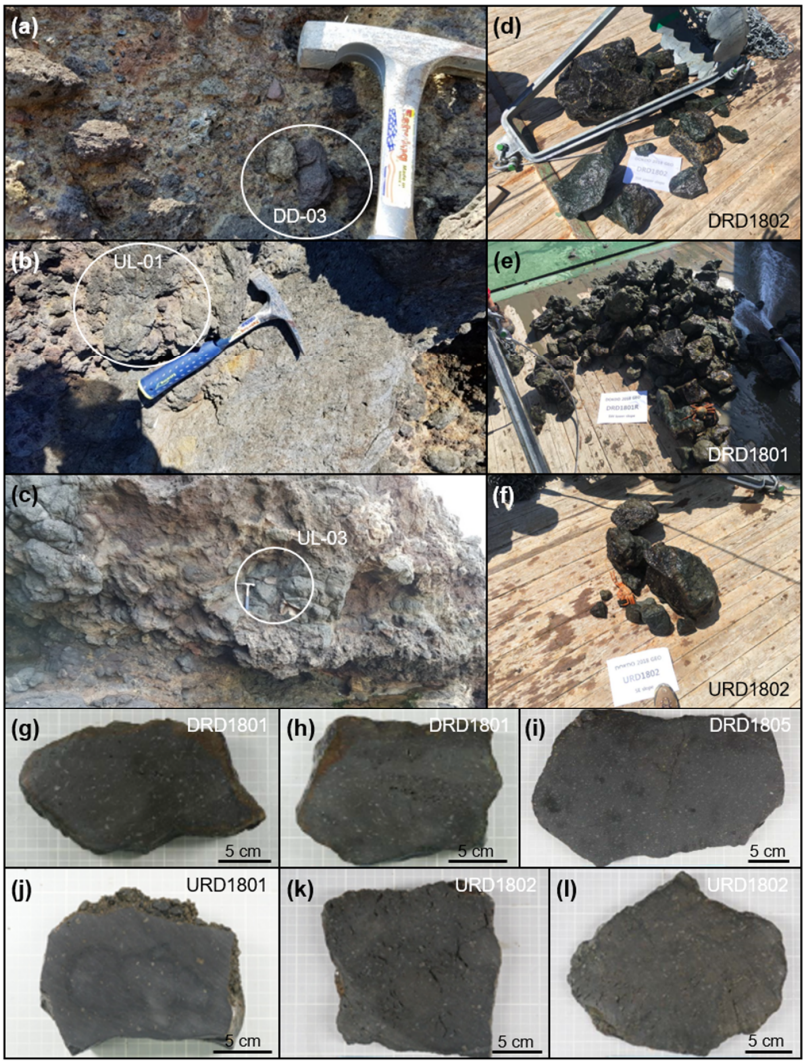

Figure 2. Photographs of terrestrial samples from (**a**) Dokdo and (**b**,**c**) Ulleung islands and submarine samples from (**d**,**e**,**g**–**i**) Dokdo and (**f**,**j**–**l**) Ulleung islands. (**a**,**d**–**l**) are trachytic rocks, whereas (**b**,**c**) are basaltic agglomerate samples. (**d**–**f**) the dredged rock samples of Onnuri R/V. The sampling location is shown in Figure 1.

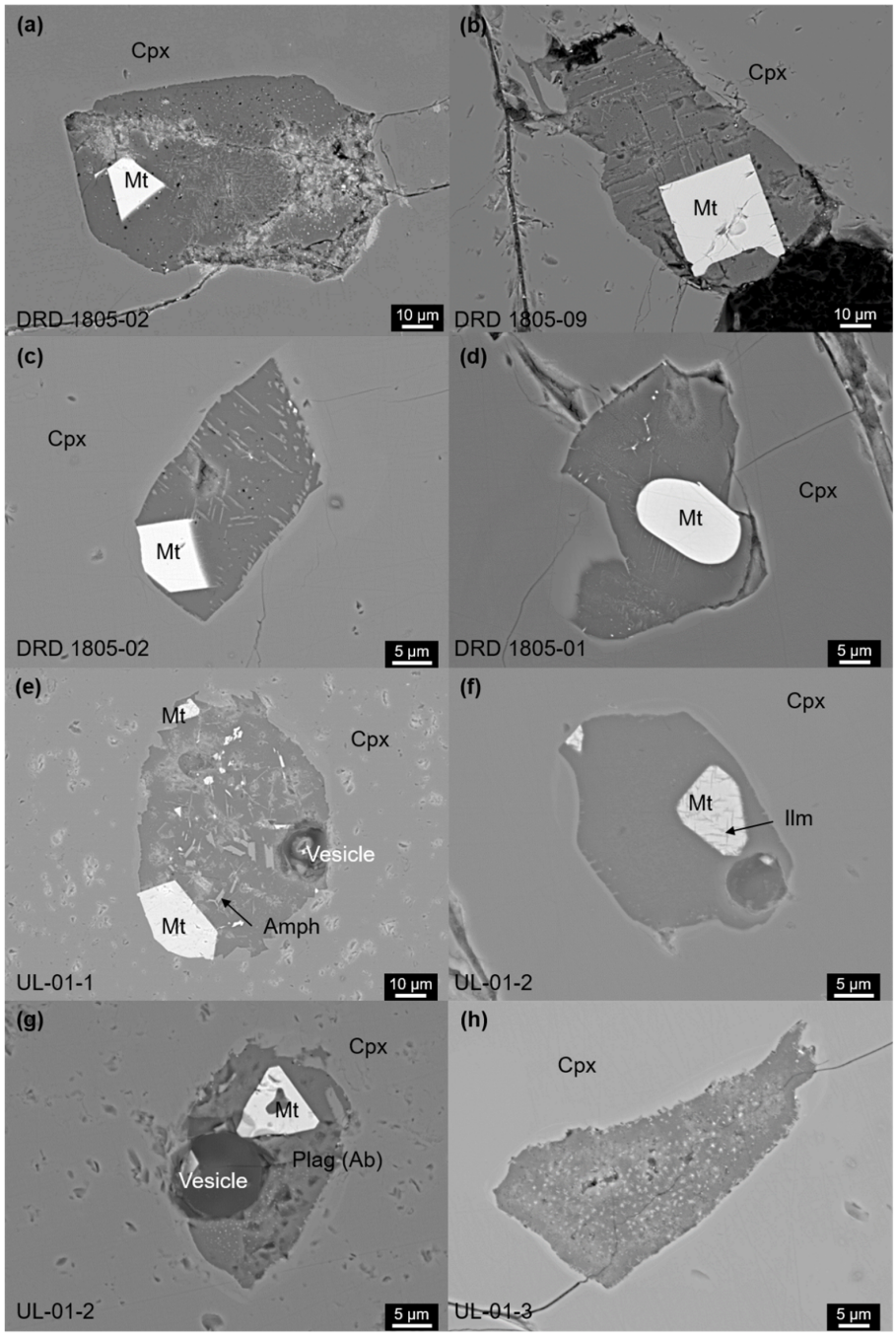

Figure 3. Backscattered-electron (BSE) images of crystallized melt inclusions hosted in clinopyroxene of trachyte from (**a**–**d**) Dokdo and (**e**–**h**) Ulleung islands. Mt: Ti-magnetite; Amph: amphibole; Cpx: clinopyroxene; Plag: plagioclase; Ilm: ilmenite.

4.2. Major-Element Geochemistry of DUI Submarine Rocks

Submarine rocks collected from the DUI region were classified as trachyte, trachyandesite, and trachybasalt according to total alkalis-versus-silica (TAS) chemical-classification diagram (Figure 4 and Table 1). Although terrestrial samples (DD-03, UL-01, UL-02, UL-03, UL-04, and UL-07) were not analyzed for major-element geochemistry, on the basis of previous studies and the geological map, it was known that DD-03 was a trachyte, and samples on Ulleung were basaltic rocks (Figure 1d,e).

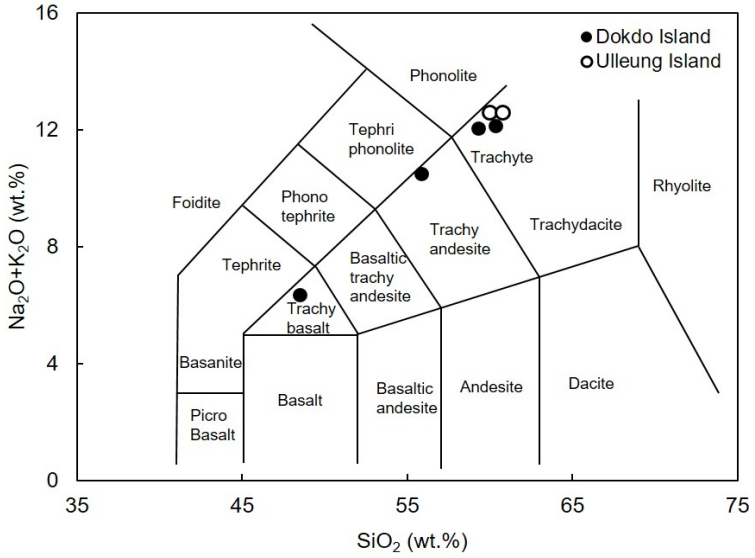

Figure 4. Total alkali–silica (TAS) diagram [49] of DUI volcanic rocks.

Table 1. Chemical compositions of trachytes from Dokdo and Ulleung islands.

Location	Dokdo Island				Ulleung Island	
Sample ID	DRD	DRD	DRD	DRD	URD	URD
	1801R-04	1804-04	1805-01	1805-02	1801-02	1802-02
SiO_2	55.8	61.1	59.3	48.5	47.4	60.9
Al_2O_3	18.5	18.2	17.7	16.0	16.0	18.0
$Fe_2O_3{}^T$	4.86	4.70	5.97	8.94	9.99	3.95
MnO	0.13	0.14	0.25	0.14	0.15	0.15
MgO	1.36	0.61	0.77	5.68	4.64	0.47
CaO	3.19	1.85	2.41	9.63	8.27	1.11
Na_2O	5.00	5.63	5.88	3.04	3.46	6.47
K_2O	5.50	6.64	6.16	3.30	3.26	6.29
TiO_2	0.95	0.40	0.59	2.72	3.47	0.09
P_2O_5	0.24	0.08	0.14	0.82	1.33	1.66
Total	95.5	99.4	99.2	99.8	98.0	99.1

4.3. Daughter-Mineral Phases

Daughter minerals in clinopyroxene phenocrysts exhibited amphibole and Ti-magnetite associations with or without irregularly shaped vesicles. The phase compositions of daughter minerals within the melt inclusions were identified by Raman spectroscopic analysis, and the most representative data are shown in Table 2. Comparable data of the representative Raman spectra by RRUFF (http://rruff.info/) and the Raman spectrum of this study are shown. The RRUFF database provides the standard Raman spectra of minerals. Inconsistencies in Raman spectra between natural and reference materials were attributed to impurities and defects in the samples, oxidation, and different sample origins [50]. The host clinopyroxene is characterized by the spectrum at 329–337, 395–397, 532–555, 663–669, 825–829, and 1005–1014 cm^{-1}. The Raman spectrum of magnetite comprised 320–324, 482, 548–561, and 673–681 cm^{-1}, and the amphibole was composed of 540–554 and 692–698 cm^{-1} (Figure 5).

Table 2. Range of Raman spectrum of representative mineral phases in this study and representative Raman spectrum from RRUFF database (cm^{-1}).

Mineral Phases	This Study	Reference Value [1]
Plagioclase	285–289, 478–487, 507–516, 561–565, 686, 985	291, 479, 507
Clinopyroxene	329–337, 395–397, 532–555, 663–669, 825–829, 1005–1014	352, 359, 389, 667, 856, 1010
Amphibole	540–554, 692–698	530–543, 659–678
Ti-Magnetite	320–324, 482, 548–561, 673–681	317–329, 480, 561–570, 676–682

[1] RRUFF database (http://rruff.info/).

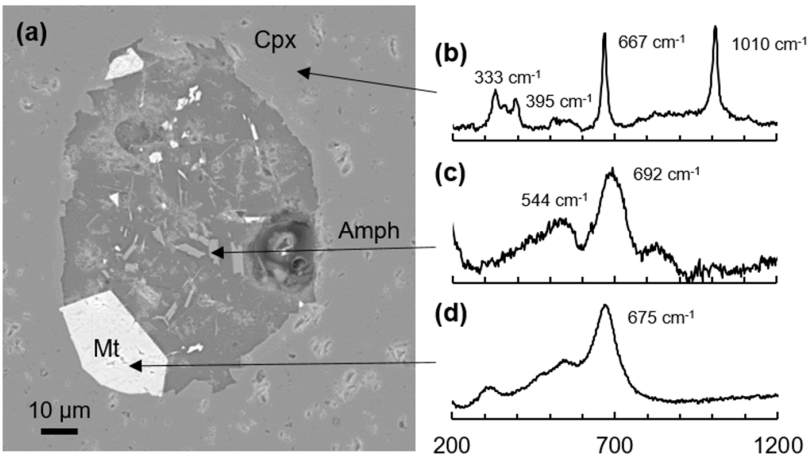

Figure 5. (**a**) BSE image (from Figure 3e) of the representative melt inclusion in Dokdo and Ulleung Islands with Raman spectrum of representative mineral phases (**b**–**d**). The melt inclusion is hosted in clinopyroxene (**b**) and consists of amphibole (**c**) and Ti-magnetite (**d**). The *y*-axis of Raman spectrum represents intensity.

4.4. Daughter-Mineral Chemistry

Chemical compositions of the daughter minerals, analyzed by EPMA and SEM, are summarized in Table 3 and Figure 6. The chemical compositions of minerals by EPMA are consistent with those of element mapping by SEM. Host clinopyroxenes consisted mainly of SiO_2 (average of 47.2 wt %), CaO (average of 22.3 wt %), MgO (average of 13.8 wt %), Al_2O_3 (average of 6.67 wt %), and FeO (average of 6.65 wt %). Furthermore, most pyroxenes were augite ($Wo_{48}En_{41}Fs_{11}$) and Mg# (Mg# = $Mg/(Mg + Fe^{2+})$) from 74 to 83. The daughter magnetite grains showed relatively high TiO_2 (average of 8.04 wt %), Al_2O_3 (average of 8.68 wt %), and MgO (average of 8.28 wt %) contents, referring to Ti-magnetite. Ilmenite lamellae were observed in some of the Ti-magnetite grains (Figure 3f). Daughter amphiboles have contents of SiO_2 (51.3–59.2 wt %), Al_2O_3 (20.1–22.9 wt %), FeO (1.42–4.76 wt %), and TiO_2 (1.39–3.00 wt %), with smaller amounts of Cr_2O_3 (average of 0.01 wt %), MnO (average of 0.08 wt %), and MgO (average of 1.10 wt %)

Table 3. Electron-probe microanalyses (EPMA) of representative mineral phases of melt inclusions in the Dokdo and Ulleung volcanic rocks.

Major Element	Ti-Magnetite (n = 28)		Pyroxene (n = 32)		Amphibole (n = 30)		Plagioclase (n = 5)	
wt %	**Avg**	**STD**	**Avg**	**STD**	**Avg**	**STD**	**Avg**	**STD**
SiO_2	0.31	0.54	47.2	1.30	56.9	1.64	51.6	1.69
TiO_2	8.04	4.21	2.25	0.50	2.11	0.38	0.79	1.14
Al_2O_3	8.68	1.50	6.67	1.10	21.35	0.65	27.1	4.19
Cr_2O_3	1.23	1.60	0.18	0.12	0.01	0.02	0.00	0.00
FeO	68.1	4.35	6.65	0.52	2.42	0.67	1.52	1.55
MnO	0.58	0.19	0.11	0.03	0.08	0.04	0.05	0.07
MgO	8.28	2.03	13.8	0.72	1.10	0.46	0.60	0.93
CaO	0.23	0.23	22.3	0.22	3.62	0.96	12.1	0.95
K_2O	0.03	0.04	0.43	0.04	5.78	1.12	1.52	1.10
Na_2O	0.03	0.05	0.01	0.01	3.25	0.74	3.52	0.87
Total	95.5	1.27	99.6	0.33	96.6	1.16	98.8	1.22

n: number of analyses; Avg: average; STD: standard deviation.

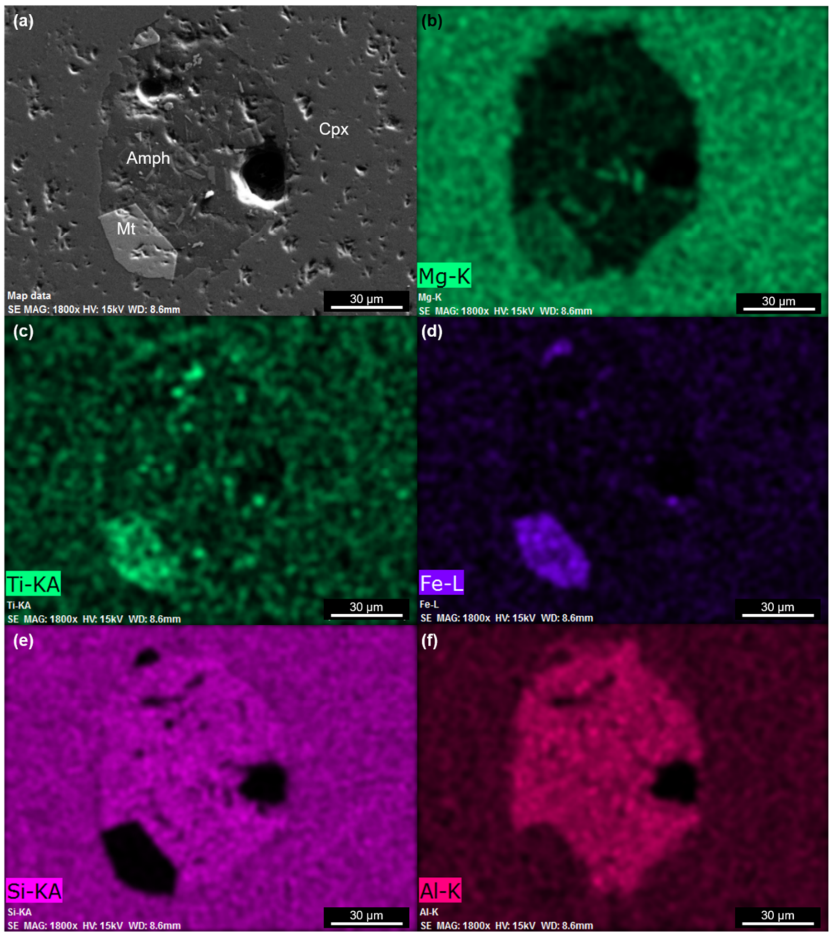

Figure 6. Element-mapping images for Mg (**b**), Ti (**c**), Fe (**d**), Si (**e**), and Al (**f**) using EDS on SEM of the representative melt inclusion (**a**). Abbreviations are same as in Figures 3 and 5.

5. Discussion

5.1. Melt Inclusions in Clinopyroxene Host

Generally, it is difficult to perform accurate quantitative elemental analysis of daughter minerals as they have small a grain size and often have the potential to interact with neighboring minerals, meaning that mineral compositional heterogeneity is inevitable (Table 3). Therefore, the measured compositions of the daughter minerals did not correspond to typical compositions of the identified phases [25]. For this reason, the identification of daughter minerals adopted the results of Raman spectroscopy and element mapping. To summarize the analytical results, the pyroxene-hosted melt inclusions were commonly composed of amphibole ± vesicle (void) ± Ti-magnetite (Figure 5). The voids were empty of low-density phases, so it was likely that melt inclusions were almost completely crystalline [51].

The precipitation of magnetite as a daughter mineral within melt inclusions can be related to diffusion. In particular, H_2O is easily re-equilibrated with the host mineral by diffusion [52–57]. Therefore, the re-equilibration between host mineral and magma results in significant H_2O loss [52,55,58]. For example, Sobolev [59] addressed that magnetite was formed inside H_2O-bearing melt inclusions under high temperatures (>1100 °C).

$$2H_2O_{melt} + 6FeO_{melt} = 2H_2\uparrow + 2Fe_3O_4$$

Or:

$$H_2O_{melt} + 2FeO_{melt} = 2H_2\uparrow + Fe_2O_{3melt}$$

As shown in these reactions, H_2O within melt inclusions can dissociate to produce H^+ diffusing out of the melt inclusions [58]. Thus, the diffusive loss of H^+ may cause excessive oxygen, leading to the oxidation of Fe^{2+} to Fe^{3+} for magnetite crystallization in melt inclusions of DUI volcanic rocks.

5.2. Geochemical Evidence of Fe–Ti-Rich Parental Magma

The volcanic-rock samples from DUI included trachybasalt, trachyandesite, and trachyte. Their compositional variability represents the significant fractional crystallization of the magma. It is generally believed that melt inclusions preserve true magmatic compositions and can be used to constrain the physical and chemical aspects of magma evolution [28]. Several scenarios can support Fe–Ti-rich parental magma for DUI volcanism. (1) Ti-Magnetite is common within melt inclusions in the clinopyroxene phenocrysts in DUI and are directly indicative of Fe-rich magma (Figure 6). Dong et al. [24] investigated melt inclusions in plagioclase from the Xinjie intrusion of the Panxi region, Southwest China, consisting of magnetite, hornblende, and apatite. They proposed that the existence of magnetite indicated Fe-rich melt. Therefore, we consider this view as insightful to assume the characteristics of melting supporting Fe-rich melt in DUI. (2) The chemical composition of magnetite provides additional evidence of Fe–Ti-rich melt [60]. The concentration of TiO_2 in Ti-magnetite shows a positive correlation with Cr_2O_3 (Figure 7), which is consistent with what was reported by Wang et al. [60]. As Fe^{3+} replaces Cr in the cubic reverse-spinel structure of magnetite, the increase in Fe reduces Cr to produce positive correlation between Cr_2O_3 and TiO_2 [61]. In addition, the identified Ti-magnetite contained a variable amount of TiO_2 of 3.57 to 17.06 wt % (average of 8.04 wt %), providing additional evidence of Fe–Ti-rich parental magma [24]. The Ti content in magnetite is controlled in the redox state [62–65], and Velasco et al. [66] argued that TiO_2 could be incorporated into magnetite through the redox state. Under oxidizing conditions, the redox system of magma enables the rapid electronic exchange between Fe-rich melt and SO_2 escape. In the end, it is allowed to exceed the formation of Fe^{3+} with chemical equilibrium. Under these conditions, a change from a redox state to higher fO_2 occurred during gas-phase release and eruption, and a high proportion of Fe^{3+} was also found in magma. As a result, Fe^{3+} could enter the octahedral site in the magnetite structure, suppressing the incorporation of Ti [67,68]. Therefore, it is proposed that Ti-magnetite in this study is formed under oxidizing conditions.

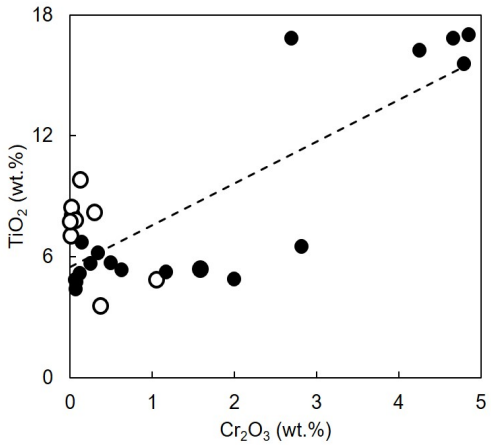

Figure 7. Plot of TiO_2 vs. Cr_2O_3 for Ti-magnetite in the Dokdo and Ulleung volcanic rocks; symbols are as in Figure 4.

There is also more evidence in the literature advocating for Fe–Ti-rich DUI primary magma. Brenna et al. [1] examined pre- and syneruptive magma styles in detail, and the evolutionary states of trachytic and phonolitic magma on the basis of the petrogenetic and geochemical signatures of Ulleung volcanic rocks. They classified volcanic rocks as trachybasaltic-to-basaltic trachyandesite lava and dykes, trachytic lava and dykes, and phonolitic pumice, and noted the occurrence of Fe oxides (magnetite and Fe–Ti magnetite) in the rocks. For example, trachybasaltic-to-basaltic trachyandesite lava and dyke samples typically contained magnetite inclusions in olivine and clinopyroxene phenocrysts. In addition, disseminated Fe–Ti oxides and magnetite inclusions were widely distributed in some euhedral-to-subhedral alkali feldspar, clinopyroxene, olivine, biotite, and plagioclase phenocrysts, and clinopyroxene groundmass. The phonolitic pumice also preserved Fe–Ti oxide inclusions both in mineral phenocrysts and groundmass. Furthermore, phaneritic lithic suites were composed of alkali feldspar, amphibole, and clinopyroxene, with minor disseminated Fe–Ti oxides, and Fe–Ti oxide inclusions found in feldspar and amphibole phenocrysts. The chemical composition of Fe–Ti oxides was variable, with relatively high concentrations of TiO_2 (5.83–48.25 wt %) and Al_2O_3 (0.13–6.39 wt %) [1]. Choi et al. [3], and Chen et al. [2] provided petrographic descriptions of magnetite phenocrysts and groundmass of the DUI volcanic rocks. Chen et al. [2] proposed fractional crystallization dominated by hornblende and titanomagnetite during DUI magma evolution. This is also supported by negative correlations between FeO^T, MgO, TiO_2, and SiO_2 and negative Ti anomalies in the spider diagrams of the DUI rocks [2]. Therefore, results are consistent with those reported in this study and may provide potential evidence of Fe–Ti-rich parent magma [24].

5.3. Conceptual Magma Evolution Model

Many studies focused on the magma-evolution processes and possible tectonic evolutionary models of DUI [1,2,69–78]. Recently, Brenna et al. [1] and Chen et al. [2] suggested geochemical evidence for the volcanic-eruption stages and the DUI magmatic plumbing system. Brenna et al. [1], for example, proposed that DUI magma has intraplate signatures and four stages of eruption history. In particular, they proposed that there are two parental-magma types (that is, trachytic and phonolitic) based on distinct geochemical/isotopic signatures and their final storage differences. Trachytic magma erupted from shallow depths and is associated with the assimilation of crustal materials and degassing, while phonolitic magma erupted from deeper levels over a short period of time without crustal contamination [1]. Chen et al. [2] proposed that the DUI magma plumbing system consisting of magma reservoirs, sills, and dikes at depths between 20 and 100 km can be used to understand the magmatic evolutionary model. As multiple eruption stages resulted from multiple magma reservoirs beneath

DUI, the volcanic rocks have a variety of petrogenetic and geochemical signatures, including distinctive isotopic signatures.

The primary magmatic-evolution processes of the DUI submarine volcanic rocks were extensively studied but remain ambiguous. Choudhary et al. [52] found that volatile dissociation processes directly affect the composition of melt inclusions, and fluid and volatile diffusion occurs in microcracks after pressure reduction in the melt inclusions and expansion of the melt, resulting in the leakage of CO_2 and H_2O from the vapor phase. This indicates that the depth of melt entrapment influences the volatile contents of the melt. In other words, melting with the presence of H_2O is closely related to tectonic setting [52]. In addition, the diffusion of hydrous components from melt inclusions leads to the crystallization of daughter minerals [58]. Therefore, diffusion processes (e.g., H_2O dissociation and H_2 loss) play a pivotal role in the magnetite precipitation of melt inclusions as an oxidation reaction when melt inclusion kept at high temperatures.

In particular, the East Sea opening was completed when the configuration of the back-arc basin (21–14 Ma) and further back-arc expansion with ongoing volcanism occurred in DUI following the trench retreat of the northwestern Pacific subducting plate [2,79]. This tectonic event resulted in a pressure gradient in magma reservoirs and can be thought as the driving force for the magma plumbing system [2]. In addition, DUI magma is known to contain 3 to 8 wt % of H_2O [19–21,80]. With the results of previously reported DUI volcanic rocks, the presence of Ti-magnetite crystals and voids in the melt inclusions of this study indicated that initial melt inclusions might be volatile-rich, reflecting hydrous primary magma. Recently, the formation of a shallow and hydrous mantle plume from the mantle transition zone (MTZ) at 410–660 km depth was suggested for the genesis of the Cenozoic alkaline basalts in northeast China [81,82]. Therefore, we suggest that the hydrous and Fe-rich characteristics of the DUI magma could have also been inherited by a similar process.

6. Conclusions

On the basis of the analytical results of melt-inclusions in the DUI volcanic rocks, the following conclusions are drawn: Melt inclusions contain Ti-magnetite crystals which were affected by diffusion. The dissociation of H_2O and diffusion of H_2 resulted in oxidizing condition and subsequent Ti-magnetite crystallization. The sufficiently hydrous material might be supplied by the magmatic plumbing system beneath DUI. In addition, the existence of Ti-magnetite in melt inclusions indicated high concentrations of Fe and Ti in the melt and/or fluids. Therefore, our results suggest that the DUI magma is hydrous and oxidized, which implies that water played a role in the melting of magma beneath the East Sea (Sea of Japan) back-arc basin in the eastern Eurasian plate.

Author Contributions: I.M. and H.L. collaboratively designed the study and wrote the manuscript; I.M. performed sample analysis; H.L., J.K., C.H.K. and C.H.P. contributed to sample acquisition; J.K., J.O., D.S. and I.L. supported analysis and manuscript writing. All authors have read and agreed to the published version of the manuscript.

Funding: This research was funded by the Ministry of Oceans and Fisheries, Korea—Sustainable Research and Development of Dokdo (PG51650).

Acknowledgments: We are grateful to the staff members of Onnuri R/V for collecting the dredge samples. We also thank the administrative staff of the East Sea Research Institute, Korea Institute of Ocean Science and Technology (KIOST).

Conflicts of Interest: The authors declare no conflict of interest.

References

1. Brenna, M.; Price, R.; Cronin, S.J.; Smith, I.E.; Sohn, Y.K.; Kim, G.B.; Maas, R. Final magma storage depth modulation of explosivity and trachyte–phonolite genesis at an intraplate volcano: A case study from Ulleung Island, South Korea. *J. Petrol.* **2014**, *55*, 709–747. [CrossRef]
2. Chen, S.S.; Lee, S.G.; Lee, T.J.; Lee, Y.S.; Liu, J.Q. Multistage magmatic plumbing system of the volcano: A case study from Ulleung Island, South Korea. *Lithos* **2018**, *314*, 201–215.

3. Choi, S.H.; Mukasa, S.B.; Kwon, S.-T.; Andronikov, A.V. Sr, Nd, Pb and Hf isotopic compositions of late Cenozoic alkali basalts in South Korea: Evidence for mixing between the two dominant asthenospheric mantle domains beneath East Asia. *Chem. Geol.* **2006**, *232*, 134–151. [CrossRef]
4. Hwang, S.K.; Hwang, J.H.; Kwon, C.W. Volcanic geology of the Ulleungdo Quadrangle. *J. Petrol. Soc. Korea* **2013**, 119–122.
5. Kim, C.H.; Park, C.H.; Jeong, E.Y.; Ko, Y.T.; Hwang, J.S.; Shim, T.M. Flexural isostasy and loading sequence of the Dokdo seamounts on the Ulleung Basin in the East Sea (Sea of Japan). *J. Asian Earth Sci.* **2009**, *35*, 459–468. [CrossRef]
6. Kim, C.H.; Park, J.W.; Lee, M.H.; Park, C.H. Detailed bathymetry and submarine terraces in the coastal area of the Dokdo volcano in the Ulleung Basin, the East Sea (Sea of Japan). *J. Coast. Res.* **2013**, 523–528. [CrossRef]
7. Kim, K. K–Ar ages and Nd–Sr isotopes of Dokdo alkali volcanic rocks in the East Sea, South Korea. *J. Geol. Soc.* **2000**, *36*, 313–324.
8. Kim, Y.; Lee, D.; Lee, K. Fractional crystallization of the volcanic rocks from Dog Island. *J. Geol. Soc.* **1987**, *23*, 67–82.
9. Lee, J.I.; Hur, S.D.; Lee, M.J.; Yoo, C.M.; Park, B.K.; Kim, Y.D.; Kwon, M.S.; Nagao, K. Petrology and Geochemistry of Dokdo Valcanic Rocks, East Sea. *Ocean Polar Res.* **2002**, *24*, 465–482. [CrossRef]
10. Shim, S.H.; Im, J.H.; Jang, Y.D.; Choo, C.O.; Park, B.J.; Kim, J.H. Petrological characteristics and origin of volcaniclasts within the Massive Tuff Breccia Formation from Dokdo Island, Korea. *J. Petrol. Soc. Korea* **2010**, *19*, 141–156.
11. Sohn, Y.; Park, K. Geology and evolution of Tok Island, Korea. *J. Geol. Soc.* **1994**, *30*, 242–261.
12. Song, Y.S.; Park, M.E.; Park, K.H. Ages and evolutions of the volcanic rocks from Ulleung-do and Dok-do. *J. Petrol. Soc. Korea* **2006**, *15*, 72–80.
13. Song, Y.; Frey, F.A.; Zhi, X. Isotopic characteristics of Hannuoba basalts, eastern China: Implications for their petrogenesis and the composition of subcontinental mantle. *Chem. Geol.* **1990**, *88*, 35–52. [CrossRef]
14. Tatsumoto, M.; Basu, A.R.; Wankang, H.; Junwen, W.; Guanghong, X. Sr, Nd, and Pb isotopes of ultramafic xenoliths in volcanic rocks of Eastern China: Enriched components EMI and EMII in subcontinental lithosphere. *Earth Planet. Sci. Lett.* **1992**, *113*, 107–128. [CrossRef]
15. Class, C.; Miller, D.M.; Goldstein, S.L.; Langmuir, C.H. Distinguishing melt and fluid subduction components in Umnak Volcanics, Aleutian Arc. *Geochem. Geophys. Geosyst.* **2000**, *1*. [CrossRef]
16. Tatsumi, Y.; Hamilton, D.; Nesbitt, R. Chemical characteristics of fluid phase released from a subducted lithosphere and origin of arc magmas: Evidence from high-pressure experiments and natural rocks. *J. Volcanol. Geotherm. Res.* **1986**, *29*, 293–309. [CrossRef]
17. Turner, S.; Caulfield, J.; Turner, M.; Van Keken, P.; Maury, R.; Sandiford, M.; Prouteau, G. Recent contribution of sediments and fluids to the mantle's volatile budget. *Nat. Geosci.* **2012**, *5*, 50–54. [CrossRef]
18. Zhang, M.; Guo, Z.; Cheng, Z.; Zhang, L.; Liu, J. Late Cenozoic intraplate volcanism in Changbai volcanic field, on the border of China and North Korea: Insights into deep subduction of the Pacific slab and intraplate volcanism. *J. Geol. Soc.* **2015**, *172*, 648–663. [CrossRef]
19. Lepage, L.D. ILMAT: An Excel worksheet for ilmenite–magnetite geothermometry and geobarometry. *Comput. Geosci.* **2003**, *29*, 673–678. [CrossRef]
20. Ridolfi, F.; Renzulli, A. Calcic amphiboles in calc–alkaline and alkaline magmas: Thermobarometric and chemometric empirical equations valid up to 1130 °C and 2.2 GPa. *Contrib. Mineral. Petrol.* **2012**, *163*, 877–895. [CrossRef]
21. Spencer, K.J.; Lindsley, D.H. A solution model for coexisting iron–titanium oxides. *Am. Mineral.* **1981**, *66*, 1189–1201.
22. Roedder, E. Origin and significance of magmatic inclusions. *Bull. Minéral.* **1979**, *102*, 487–510. [CrossRef]
23. Berlo, K.; Stix, J.; Roggensack, K.; Ghaleb, B. A tale of two magmas, Fuego, Guatemala. *Bull. Volcanol.* **2012**, *74*, 377–390. [CrossRef]
24. Dong, H.; Xing, C.; Wang, C.Y. Textures and mineral compositions of the Xinjie layered intrusion, SW China: Implications for the origin of magnetite and fractionation process of Fe–Ti-rich basaltic magmas. *Geosci. Front.* **2013**, *4*, 503–515. [CrossRef]

25. Sekisova, V.; Sharygin, V.; Zaitsev, A.; Strekopytov, S. Liquid immiscibility during crystallization of forsterite–phlogopite ijolites at Oldoinyo Lengai Volcano, Tanzania: Study of melt inclusions. *Russ. Geol. Geophys.* **2015**, *56*, 1717–1737. [CrossRef]
26. Jennings, E.S.; Gibson, S.A.; Maclennan, J.; Heinonen, J.S. Deep mixing of mantle melts beneath continental flood basalt provinces: Constraints from olivine-hosted melt inclusions in primitive magmas. *Geochim. Cosmochim. Acta* **2017**, *196*, 36–57. [CrossRef]
27. Rowe, M.C.; Nielsen, R.L.; Kent, A.J. Anomalously high Fe contents in rehomogenized olivine-hosted melt inclusions from oxidized magmas. *Am. Mineral.* **2006**, *91*, 82–91. [CrossRef]
28. Korsakov, A.V.; Golovin, A.V.; De Gussem, K.; Sharygin, I.S.; Vandenabeele, P. First finding of burkeite in melt inclusions in olivine from sheared lherzolite xenoliths. *Spectrochim. Acta Part A Mol. Biomol. Spectrosc.* **2009**, *73*, 424–427. [CrossRef] [PubMed]
29. Uyeda, S.; Miyashiro, A. Plate tectonics and the Japanese Islands: A synthesis. *Geol. Soc. Am. Bull.* **1974**, *85*, 1159–1170. [CrossRef]
30. Uto, K.; Takahashi, E.; Nakamura, E.; Kaneoka, I. Geochronology of alkali volcanism in Oki-Dogo Island, southwest Japan: Geochemical evolution of basalts related to the opening of the Japan Sea. *Geochem. J.* **1994**, *28*, 431–449. [CrossRef]
31. Fournier, M.; Jolivet, L.; Fabbri, O. Neogene stress field in SW Japan and mechanism of deformation during the Sea of Japan opening. *J. Geophys. Res. Solid Earth* **1995**, *100*, 24295–24314. [CrossRef]
32. Jolivet, L.; Shibuya, H.; Fournier, M. Paleomagnetic rotations and the Japan Sea opening. *Geophys. Monogr.* **1995**, *88*, 355–369.
33. Jolivet, L.; Tamaki, K.; Fournier, M. Japan Sea, opening history and mechanism: A synthesis. *J. Geophys. Res. Solid Earth* **1994**, *99*, 22237–22259. [CrossRef]
34. Kim, H.-J.; Lee, G.H.; Jou, H.-T.; Cho, H.-M.; Yoo, H.-S.; Park, G.-T.; Kim, J.-S. Evolution of the eastern margin of Korea: Constraints on the opening of the East Sea (Japan Sea). *Tectonophysics* **2007**, *436*, 37–55. [CrossRef]
35. Lee, G.H.; Kim, H.J.; Suh, M.C.; Hong, J.K. Crustal structure, volcanism, and opening mode of the Ulleung Basin, East Sea (Sea of Japan). *Tectonophysics* **1999**, *308*, 503–525. [CrossRef]
36. Otofuji, Y.-I.; Matsuda, T.; Nohda, S. Opening mode of the Japan Sea inferred from the palaeomagnetism of the Japan Arc. *Nature* **1985**, *317*, 603. [CrossRef]
37. Tamaki, K. Tectonic synthesis and implications of Japan Sea ODP drilling. *Proc. ODP Sci. Results* **1992**, *127*, 1333–1348.
38. Ingle, C. Subsidence of the Japan Sea: Stratigraphic evidence from ODP sites and onshore sections. *Proc. ODP Sci. Results* **1992**, *127*, 1–197.
39. Yoon, S.; Chough, S. Regional strike slip in the eastern continental margin of Korea and its tectonic implications for the evolution of Ulleung Basin, East Sea (Sea of Japan). *Geol. Soc. Am. Bull.* **1995**, *107*, 83–97. [CrossRef]
40. Yoon, S.; Sohn, Y.; Chough, S. Tectonic, sedimentary, and volcanic evolution of a back-arc basin in the East Sea (Sea of Japan). *Mar. Geol.* **2014**, *352*, 70–88. [CrossRef]
41. Fisher, R.V.; Schmincke, H.U. Alteration of volcanic glass. In *Pyroclastic Rocks*; Springer: Berlin/Heidelberg, Germany, 1984; pp. 312–345.
42. Moore, J.G.; Fiske, R.S. Volcanic substructure inferred from dredge samples and ocean-bottom photographs, Hawaii. *Geol. Soc. Am. Bull.* **1969**, *80*, 1191–1202. [CrossRef]
43. Sohn, Y. Geology of Tok Island, Korea: Eruptive and depositional processes of a shoaling to emergent island volcano. *Bull. Volcanol.* **1995**, *56*, 660–674. [CrossRef]
44. Kim, K. Petrology of Ulreung islands, Korea-Part 2, Petrography and bulk chemical composition. *J. Petrol. Mineral. Econ. Geol.* **1985**, *80*, 292–303. [CrossRef]
45. Kim, Y. Petrology of Ulreung island, Korea—Part 1, Geology. *J. Petrol. Mineral. Econ. Geol.* **1985**, *80*, 128–135. [CrossRef]
46. Xu, S.; Uto, K.; Kim, Y.K. K-Ar dating of volcanic rocks from Ulreung Island, Korea. *Geochem. J.* **1998**, *32*, 117–123. [CrossRef]
47. Golovin, A.; Sharygin, V.; Pokhilenko, N. Melt inclusions in olivine phenocrysts in unaltered kimberlites from the Udachnaya-East pipe, Yakutia: Some aspects of kimberlite magma evolution during late crystallization stages. *Petrology* **2007**, *15*, 168–183. [CrossRef]
48. Nielsen, R.L.; Michael, P.J.; Sours-Page, R. Chemical and physical indicators of compromised melt inclusions. *Geochim. Cosmochim. Acta* **1998**, *62*, 831–839. [CrossRef]

49. Bas, M.L.; Maitre, R.L.; Streckeisen, A.; Zanettin, B. A chemical classification of volcanic rocks based on the total alkali–silica diagram. *J. Petrol.* **1986**, *27*, 745–750. [CrossRef]
50. Shebanova, O.N.; Lazor, P. Raman spectroscopic study of magnetite ($FeFe_2O_4$): A new assignment for the vibrational spectrum. *J. Solid State Chem.* **2003**, *174*, 424–430. [CrossRef]
51. Manley, C.R. Morphology and maturation of melt inclusions in quartz phenocrysts from the Badlands rhyolite lava flow, southwestern Idaho. *Am. Mineral.* **1996**, *81*, 158–168. [CrossRef]
52. Choudhary, B.R.; Santosh, M.; De Vivo, B.; Jadhav, G.; Babu, E. Melt inclusion evidence for mantle heterogeneity and magma degassing in the Deccan large Igneous Province, India. *Lithos* **2019**, *346*, 105135. [CrossRef]
53. Danushevsky, L.V.; Eggins, S.M.; Falloon, T.J.; Christie, D.M. H_2O abundance in depleted to moderately enriched mid-ocean ridge magmas; Part I: Incompatible behaviour, implications for mantle storage, and origin of regional variations. *J. Petrol.* **2000**, *41*, 1329–1364. [CrossRef]
54. Gaetani, G.A.; Watson, E.B. Open system behavior of olivine-hosted melt inclusions. *Earth Planet. Sci. Lett.* **2000**, *183*, 27–41. [CrossRef]
55. Sobolev, A.V.; Chaussidon, M. H_2O concentrations in primary melts from supra-subduction zones and mid-ocean ridges: Implications for H_2O storage and recycling in the mantle. *Earth Planet. Sci. Lett.* **1996**, *137*, 45–55. [CrossRef]
56. Sobolev, A.V.; Danyushevsky, L.V. Petrology and geochemistry of boninites from the north termination of the Tonga Trench: Constraints on the generation conditions of primary high-Ca boninite magmas. *J. Petrol.* **1994**, *35*, 1183–1211. [CrossRef]
57. Gaetani, G.A.; O'Leary, J.A.; Shimizu, N.; Bucholz, C.E.; Newville, M. Rapid reequilibration of H_2O and oxygen fugacity in olivine-hosted melt inclusions. *Geology* **2012**, *40*, 915–918. [CrossRef]
58. Danyushevsky, L.V.; McNeill, A.W.; Sobolev, A.V. Experimental and petrological studies of melt inclusions in phenocrysts from mantle-derived magmas: An overview of techniques, advantages and complications. *Chem. Geol.* **2002**, *183*, 5–24. [CrossRef]
59. Sobolev, A. Origin of Siberian Meimechites in Relation to the General Problem of Ultramafic Magma. Ph.D. Thesis, Vernadsky Inst. of Geochemistry Moscow, USSR, Moscow, Russian, 1983.
60. Wang, C.Y.; Zhou, M.F.; Zhao, D. Fe–Ti–Cr oxides from the Permian Xinjie mafic–ultramafic layered intrusion in the Emeishan large igneous province, SW China: Crystallization from Fe-and Ti-rich basaltic magmas. *Lithos* **2008**, *102*, 198–217. [CrossRef]
61. Nadoll, P.; Angerer, T.; Mauk, J.L.; French, D.; Walshe, J. The chemistry of hydrothermal magnetite: A review. *Ore. Geol. Rev.* **2014**, *61*, 1–32. [CrossRef]
62. Andersen, J.C.; Rasmussen, H.; Nielsen, T.F.; Ronsbo, J.G. The Triple Group and the Platinova gold and palladium reefs in the Skaergaard Intrusion; stratigraphic and petrographic relations. *Econ. Geol.* **1998**, *93*, 488–509. [CrossRef]
63. Hawley, J. The Sudbury ores, their mineralogy and origin; Part 3, Interpretations; The history and origin of the Sudbury ores. *Can. Mineral.* **1962**, *7*, 146–207.
64. Jakobsen, J.K.; Veksler, I.; Tegner, C.; Brooks, C.K. Immiscible iron-and silica-rich melts in basalt petrogenesis documented in the Skaergaard intrusion. *Geology* **2005**, *33*, 885–888. [CrossRef]
65. Naldrett, A. A portion of the system Fe–S–O between 900 and 1080 C and its application to sulfide ore magmas. *J. Petrol.* **1969**, *10*, 171–201. [CrossRef]
66. Velasco, F.; Tornos, F.; Hanchar, J.M. Immiscible iron-and silica-rich melts and magnetite geochemistry at the El Laco volcano (northern Chile): Evidence for a magmatic origin for the magnetite deposits. *Ore Geol. Rev.* **2016**, *79*, 346–366. [CrossRef]
67. Jugo, P.J.; Luth, R.W.; Richards, J.P. An experimental study of the sulfur content in basaltic melts saturated with immiscible sulfide or sulfate liquids at 1300 °C and 1·0 GPa. *J. Petrol.* **2005**, *46*, 783–798. [CrossRef]
68. Kelley, K.A.; Cottrell, E. The influence of magmatic differentiation on the oxidation state of Fe in a basaltic arc magma. *Earth Planet. Sci. Lett.* **2012**, *329*, 109–121. [CrossRef]
69. Anderson, D.L.; Tanimoto, T.; Zhang, Y.-S. Plate tectonics and hotspots: The third dimension. *Science* **1992**, *256*, 1645–1651. [CrossRef]
70. Basu, A.R.; Junwen, W.; Wankang, H.; Guanghong, X.; Tatsumoto, M. Major element, REE, and Pb, Nd and Sr isotopic geochemistry of Cenozoic volcanic rocks of eastern China: Implications for their origin from suboceanic-type mantle reservoirs. *Earth Planet. Sci. Lett.* **1991**, *105*, 149–169. [CrossRef]

71. Chung, S.-L.; Jahn, B.-M.; Chen, S.-J.; Lee, T.; Chen, C.-H. Miocene basalts in northwestern Taiwan: Evidence for EM-type mantle sources in the continental lithosphere. *Geochim. Cosmochim. Acta* **1995**, *59*, 549–555. [CrossRef]
72. Chung, S.-L.; Sun, S.-S.; Tu, K.; Chen, C.-H.; Lee, C.-Y. Late Cenozoic basaltic volcanism around the Taiwan Strait, SE China: Product of lithosphere–asthenosphere interaction during continental extension. *Chem. Geol.* **1994**, *112*, 1–20. [CrossRef]
73. Lee, M.W. Petrology and geochemistry of Jeju volcanic island, Korea. *Sci. Rep. Tohoku Univ. Ser. 3* **1982**, *15*, 177–256.
74. Nakamura, E.; Campbell, I.H.; McCulloch, M.T.; Sun, S.S. Chemical geodynamics in a back arc region around the Sea of Japan: Implications for the genesis of alkaline basalts in Japan, Korea, and China. *J. Geophys. Res. Solid Earth* **1989**, *94*, 4634–4654. [CrossRef]
75. Park, J. Petrology and petrogenesis of the Cenozoic alkali volcanic rocks in the middle part of Korean Peninsula (I): Petrography, mineral chemistry and whole rock majo element chemistry. *J. Gent. Soc. Korea* **1996**, *32*, 223–249.
76. Tu, K.; Flower, M.F.; Carlson, R.W.; Xie, G.; Chen, C.-Y.; Zhang, M. Magmatism in the South China Basin: 1. Isotopic and trace-element evidence for an endogenous Dupal mantle component. *Chem. Geol.* **1992**, *97*, 47–63. [CrossRef]
77. Tu, K.; Flower, M.F.; Carlson, R.W.; Zhang, M.; Xie, G. Sr, Nd, and Pb isotopic compositions of Hainan basalts (south China): Implications for a subcontinental lithosphere Dupal source. *Geology* **1991**, *19*, 567–569. [CrossRef]
78. Zhou, X.-H.; Zhu, B.-Q.; Liu, R.-X.; Chen, W.-J. Cenozoic basaltic rocks in eastern China. In *Continental Flood Basalts*; Springer: Berlin/Heidelberg, Germany, 1988; pp. 311–330.
79. Nohda, S. Formation of the Japan Sea basin: Reassessment from Ar–Ar ages and Nd–Sr isotopic data of basement basalts of the Japan Sea and adjacent regions. *J. Asian. Earth Sci.* **2009**, *34*, 599–609. [CrossRef]
80. TsuBoI, S. On the genesis of leucite rock of Island Utsuryoto (Ullungdo, Korea). *Proc. Jpn. Acad. Ser. B* **1981**, *57*, 233–238. [CrossRef]
81. Yang, J.; Faccenda, M. Intraplate volcanism originating from upwelling hydrous mantle transition zone. *Nature* **2020**, *579*, 88–91. [CrossRef]
82. Kuritani, T.; Xia, Q.-K.; Kimura, J.-I.; Liu, J.; Shimizu, K.; Ushikubo, T.; Zhao, D.; Nakagawa, M.; Yoshimura, S. Buoyant hydrous mantle plume from the mantle transition zone. *Sci. Rep.* **2019**, *9*, 1–7. [CrossRef]

© 2020 by the authors. Licensee MDPI, Basel, Switzerland. This article is an open access article distributed under the terms and conditions of the Creative Commons Attribution (CC BY) license (http://creativecommons.org/licenses/by/4.0/).